第 35 卷第 5 期 无 机 化 学 学 报 Vol.35 No.5
2019 年 5 月 CHINESE JOURNAL OF INORGANIC CHEMISTRY 901-909

五个吡嗪缩氨基硫脲过渡金属配合物的合成、结构和荧光性质

高亮亮[1] 黄山秀*,[1] 康瑞芳[1] 代耿耿[1] 吴伟娜[1] 王 元[1] 陈 忠*,[2]
([1]河南理工大学化学化工学院,河南省煤炭绿色转化重点实验室,焦作 454000)
([2]江西科技师范大学材料与机电学院,南昌 330013)

摘要:合成并通过单晶衍射、元素分析及红外光谱表征了配合物[NiL_2] (**1**),[$Zn(HL)_2$](NO_3)$_2$ (**2**),[$Cd(HL)_2$](NO_3)$_2$ (**3**),[$Cu_2L_2(NO_3)_2$] (**4**)和[$Cu_2(L)_2(SO_4)$]·4CH_3OH (**5**)的结构(HL 为 2-乙酰-3-甲基吡嗪-缩 *N*-乙基氨基硫脲)。单晶衍射结果表明,配合物 **1** 中,Ni(Ⅱ)离子中心与 2 个脱氢的缩氨基硫脲配体中的 N_2S 供体配位,形成扭曲的八面体配位构型。在配合物 **2** 和 **3** 中,中心 Zn(Ⅱ)和 Cd(Ⅱ)离子与配合物 **1** 中 Ni(Ⅱ)离子配位构型相同,但缩氨基硫脲为三齿中性配体。而配合物 **4** 和 **5** 中均存在双核的 Cu_2S_2 中心,每个 Cu(Ⅱ)均采取扭曲的四方锥配位构型,所不同的是外轴向配位点分别由单齿配位的硝酸根和 μ_2-桥联的硫酸根所占据。此外,荧光光谱表明配合物 **1**~**5** 与 DNA 的相互作用强于配体。

关键词:晶体结构;荧光;吡嗪;缩氨基硫脲;过渡金属配合物
中图分类号:O614.81+3;O614.24+1;O614.24+1;O614.121 **文献标识码**:A **文章编号**:1001-4861(2019)05-0901-09
DOI:10.11862/CJIC.2019.065

Crystal Structures and Fluorescence Properties of Five Transition Metal Complexes with Pyrazine Thiosemicarbazone

GAO Liang-Liang[1] HUANG Shan-Xiu*,[1] KANG Rui-Fang[1]
DAI Geng-Geng[1] WU Wei-Na[1] WANG Yuan[1] CHEN Zhong*,[2]
([1]*College of Chemistry and Chemical Engineering, Henan Key Laboratory of Coal Green Conversion, Henan Polytechnic University, Jiaozuo, Henan* 454000, *China*)
([2]*School of Materials and Mechanical and Electrical Engineering, Jiangxi Science and Technology Normal University, Nanchang* 330013, *China*)

Abstract: Five transition metal complexes, [NiL_2] (**1**), [$Zn(HL)_2$](NO_3)$_2$ (**2**), [$Cd(HL)_2$](NO_3)$_2$ (**3**), [$Cu_2L_2(NO_3)_2$] (**4**) and [$Cu_2(L)_2(SO_4)$]·4CH_3OH (**5**) based on HL (HL=3-methyl-2-acetylpyrazine *N*(4)-ethylthiosemicarbazone) have been synthesized and structurally determined by single-crystal X-ray diffraction, elemental analysis and IR spectroscopy. X-ray diffraction analysis results show that the Ni(Ⅱ) ion in complex **1** with a distorted octahedron geometry is surrounded by two neutral thiosemicarbazone (TSC) ligand with N_2S donor set. On the contrary, the ligand TSC is deprotonated in the complexes **2** and **3**, although the Zn(Ⅱ) and Cd(Ⅱ) ions possess similar coordination geometry as that of Ni(Ⅱ) in complex **1**. The dimeric Cu_2S_2 cores are found in complexes **4** and **5**, and each of the Cu(Ⅱ) adopted a distorted square pyramid coordination geometry. The outer axial sites are occupied by two monodentate NO_3^- and a μ_2-SO_4^{2-} in complexes **4** and **5**, respectively. In addition, the fluorescence spectra indicate that the interactions of complexes with DNA are stronger than that of ligand HL. CCDC: 1434105, HL; 1434106, **1**; 1434107, **2**; 1434108, **3**; 1434109, **4**; 1434110, **5**.

Keywords: crystal structure; fluorescence; pyrazine; thiosemicarbazone; transition metal complex

收稿日期:2018-12-01。收修改稿日期:2019-01-02。
国家自然科学基金(No.21001040),河南省自然科学基金(No.182300410183,162300410011),江西省自然科学基金(No.20181BAB206011),河南省教育厅高等学校重点科研基金(No.19A150001),江西省教育厅科学技术研究项目(No.GJJ170665),河南理工大学校内基金(No.T2018-3,J2015-4)和江西科技师范大学校内基金(No.2015QNBJRC006)资助。
*通信联系人。E-mail:953854991@qq.com,chenzhonglzu@hotmail.com

In the past few decades, thiosemicarbazones (TSCs) and their metal complexes have been brought to focus for their biological and pharmaceutical properties [1]. As one of the most promising systems, the transition metal complexes of TSCs derived from 2-acylpyridine/2-acylpyrazine have been extensively investigated as potential anticancer agents[2-8]. It has been demonstrated that the biological activities of TSCs-metals complexes depend on not only the metal centers but also the structures of the ligands[9-12]. Moreover, to the best of our knowledge, the investigations on the transition metal complexes of TSCs derived from substituted 2-acetylpyrazine are relatively scarce[13]. Herein, three mononuclear and two binuclear transition metal complexes of the TSC ligand (HL, Scheme 1) derived from 3-methyl-2-acetylpyrazine and *N*(4)-ethylthiosemicarbazide were synthesized in this work. In addition, DNA-binding properties of the six compounds were discussed in detail.

1 Experimental

1.1 Materials and measurements

Solvents and starting materials for synthesis were purchased commercially and used as received. Elemental analysis was carried out on an Elemental Vario EL analyzer. The IR spectra (ν=4 000~400 cm^{-1}) were determined by KBr pressed disc method on a Bruker V70 FT-IR spectrophotometer. ^1H NMR spectra of HL was acquired with Bruker AV400 NMR instrument in $CDCl_3$ solution with TMS as internal standard. The UV spectra were recorded on a Purkinje General TU-1800 spectrophotometer. The interactions between six compounds and ct-DNA are measured using literature method [14] via emission spectra on a Varian CARY Eclipse spectrophotometer with the pass width of emission and excitation being 5 nm.

1.2 Preparations of the ligand and complexes 1~5

As shown in Scheme 1, a mixture of 3-methyl-2-acetylpyrazine (1.36 g, 10 mmol) and *N*(4)-ethylthiosemicarbazide (1.20 g, 10 mmol) in ethanol (30 mL) were stirred for 4 h at room temperature. The white precipitates were filtered and washed three times by cold ethanol. Yield: 1.66 g (70%). Elemental analysis Calcd. for $C_{10}H_{15}N_5S$(%): C: 50.61; H: 6.37; N: 29.51. Found(%): C: 50.47; H: 6.52; N: 29.44. ^1H NMR (400 MHz, $CDCl_3$): δ 8.77 (1H) / 8.52 (1H) for Ar-H, 8.46~8.47 (1H, d, NH), 7.44 (1H, s, NH), 3.73~3.80 (2H, m, CH_2), 2.83 (3H, s, CH_3), 2.40 (3H, s, CH_3), 1.28~1.32 (3H, t, CH_3-CH_2). FT-IR (KBr, cm^{-1}): $\nu_{N=C}$ 1 608, $\nu_{N=C}$ (pyrazine) 1 553, $\nu_{S=C}$ 813. Suitable crystals for X-ray diffraction measurement were obtained by recrystallization of HL from methanol solution.

Complexes **1** ~**5** were synthesized by reacting HL (0.5 mmol) with $Ni(OAc)_2$, $Zn(NO_3)_2$, $Cd(NO_3)_2$, $Cu(NO_3)_2$ and $CuSO_4$ (molar ratio of ligand to metal=1∶1) in methanol (20 mL) solution at room temperature, respectively. The crystals suitable for X-ray diffraction analysis were generated by evaporating the corresponding reaction solutions at room temperature.

1: Brown blocks. Yield: 52%. Anal. Calcd. for $C_{20}H_{28}N_{10}S_2Ni$(%): C, 45.21; H, 5.31; N, 26.36. Found (%): C, 45.02; H, 5.44; N, 26.24. FT-IR (KBr, cm^{-1}): $\nu_{N=C}$ 1 574, $\nu_{N=C}$(pyrazine) 1 535, $\nu_{S=C}$ 791.

2: Yellow blocks. Yield: 61%. Anal. Calcd. for $C_{20}H_{30}N_{12}O_6S_2Zn$(%): C, 36.17; H, 4.55; N, 25.31. Found (%): C, 35.98; H, 4.62; N, 25.41. FT-IR (KBr, cm^{-1}): $\nu_{N=C}$ 1 571, $\nu_{N=C}$(pyrazine) 1 533, ν (NO_3) 1 384, $\nu_{S=C}$ 791.

3: Yellow blocks. Yield: 68%. Anal. Calcd. for $C_{20}H_{30}N_{12}O_6S_2Cd$(%): C, 33.78; H, 4.25; N, 23.64. Found(%): C, 33.94; H, 4.30; N, 23.50. FT-IR (KBr, cm^{-1}): $\nu_{N=C}$ 1 573, $\nu_{N=C}$(pyrazine) 1 536, ν(NO_3) 1 383, $\nu_{S=C}$ 783.

4: Brown blocks. Yield: 53%. Anal. Calcd. for $C_{20}H_{28}N_{12}O_6S_2Cu_2$(%): C, 33.19; H, 3.90; N, 23.22. Found(%): C, 33.44; H, 3.69; N, 23.41. FT-IR (KBr, cm^{-1}): $\nu_{N=C}$ 1 576, $\nu_{N=C}$(pyrazine) 1 537, ν_1(NO_3) 1 474,

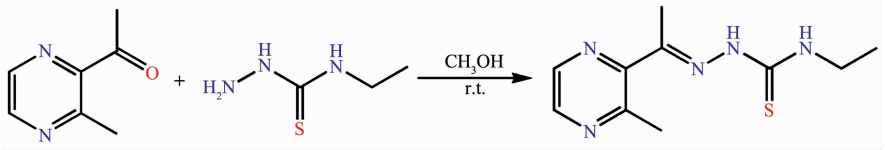

Scheme 1 Synthetic route of TSC ligand HL

$\nu_4(NO_3)$ 1 343, $\nu_{S=C}$ 795.

5: Brown blocks. Yield: 59%. Anal. Calcd. for $C_{24}H_{44}N_{10}O_8S_3Cu_2$(%): C, 34.98; H, 5.38; N, 17.00. Found(%): C, 34.79; H, 5.22; N, 17.21. FT-IR (KBr, cm^{-1}): $\nu_{N=C}$ 1 593, $\nu_{N=C}$(pyrazine) 1 536, $\nu_{S=C}$ 795.

1.3 X-ray crystallography

The X-ray diffraction measurement for HL and complexes **1**~**5** was performed on a Bruker SMART APEX Ⅱ CCD diffractometer equipped with a graphite monochromatized Mo $K\alpha$ radiation (λ=0.071 073 nm) by using φ-ω scan mode. Semi-empirical absorption correction was applied to the intensity data using SADABS program[15]. The structures were solved by direct methods and refined by full matrix least-square on F^2 using SHELXTL-97 program[16]. All non-hydrogen atoms were refined anisotropically. All H atoms were positioned geometrically and refined using a riding model. Details of the crystal parameters, data collection and refinements are summarized in Table 1.

CCDC: 1434105, HL; 1434106, **1**; 1434107, **2**; 1434108, **3**; 1434109, **4**; 1434110, **5**.

Table 1　Crystal data and structure refinement for HL and complexes 1~5

	HL	1	2	3	4	5
Empirical formula	$C_{10}H_{15}N_5S$	$C_{20}H_{28}N_{10}S_2Ni$	$C_{20}H_{30}N_{12}O_6S_2Zn$	$C_{20}H_{30}N_{12}O_6S_2Cd$	$C_{20}H_{28}N_{12}O_6S_2Cu_2$	$C_{24}H_{44}N_{10}O_8S_3Cu_2$
Formula weight	237.33	531.35	664.05	711.08	723.74	823.95
T / K	296(2)	296(2)	296(2)	296(2)	296(2)	293(2)
Crystal system	Triclinic	Monoclinic	Monoclinic	Monoclinic	Monoclinic	Monoclinic
Space group	$P\bar{1}$	$P2_1/c$	$C2/c$	$C2/c$	$C2/c$	$P2_1/c$
a / nm	0.786 6(4)	1.559 4(2)	4.544 5(9)	4.627 9(15)	1.782 2(2)	1.497 1(6)
b / nm	0.793 4(5)	1.426 9(2)	0.877 96(19)	0.878 1(3)	1.519 19(17)	1.607 4(7)
c / nm	1.087 8(6)	2.649 1(3)	1.495 7(3)	1.475 1(5)	1.333 5(3)	2.148 7(6)
α / (°)	71.625(10)					
β / (°)	76.991(10)	124.028(7)	105.464(4)	105.093(5)	127.006(2)	134.036(17)
γ / (°)	73.861(11)					
V / nm^3	0.611 8(6)	4.885 2	5.752(2)	5.788(3)	2.883 2(8)	3.717(2)
Z	2	8	8	8	4	4
D_c / ($g\cdot cm^{-3}$)	1.288	1.445	1.534	1.623	1.667	1.472
R_{int}	0.019 3	0.056 9	0.056 6	0.037 1	0.061 3	0.161 3
GOF	1.014	1.016	0.998	1.015	1.024	1.034
R indices [$I>2\sigma(I)$]	R_1=0.043 7, wR_2=0.088 2	R_1=0.043 6, wR_2=0.091 7	R_1=0.046 7, wR_2=0.089 7	R_1=0.038 3, wR_2=0.093 0	R_1=0.046 2, wR_2=0.085 4	R_1=0.071 2, wR_2=0.139 4
R indices (all data)	R_1=0.078 7, wR_2=0.101 9	R_1=0.088 4, wR_2=0.109 3	R_1=0.086 9, wR_2=0.110 8	R_1=0.053 2, wR_2=0.105 0	R_1=0.090 0, wR_2=0.101 7	R_1=0.145 0, wR_2=0.168 5

2 Results and discussion

2.1 Crystal structures description

The diamond drawings of HL and complexes **1**~**5** are shown in Fig.1 and 2. Selected bond distances and angles are listed in Table 2. Hydrogen bond parameters are listed in Table 3. The bond length of C=S in free ligand is 0.168 0(2) nm, which is slightly shorter than that in complexes **2** and **3** (0.168 5(5)~0.169 5(4) nm), showing that the TSC ligand is neutral in both complexes[17]. On the contrary, the enolization of C=S in complexes **1**, **4** and **5** can be confirmed by the bond lengths of C-S in a range of 0.172 1(8)~0.175 6(4) nm, which are in excellent agreement with other previously known acylhydrazone complexes in the literature[17]. In the crystal of HL, the molecules are linked into centrosymmetric dimers by pair of intermolecular N–H⋯O hydrogen bonds, forming a $R_2^2(10)$ ring motif.

As shown in Fig.1a, **1** is built of two independent neutral mononuclear molecules in the unit cell. Each Ni(Ⅱ) center is surrounded by two mono-anionic TSC

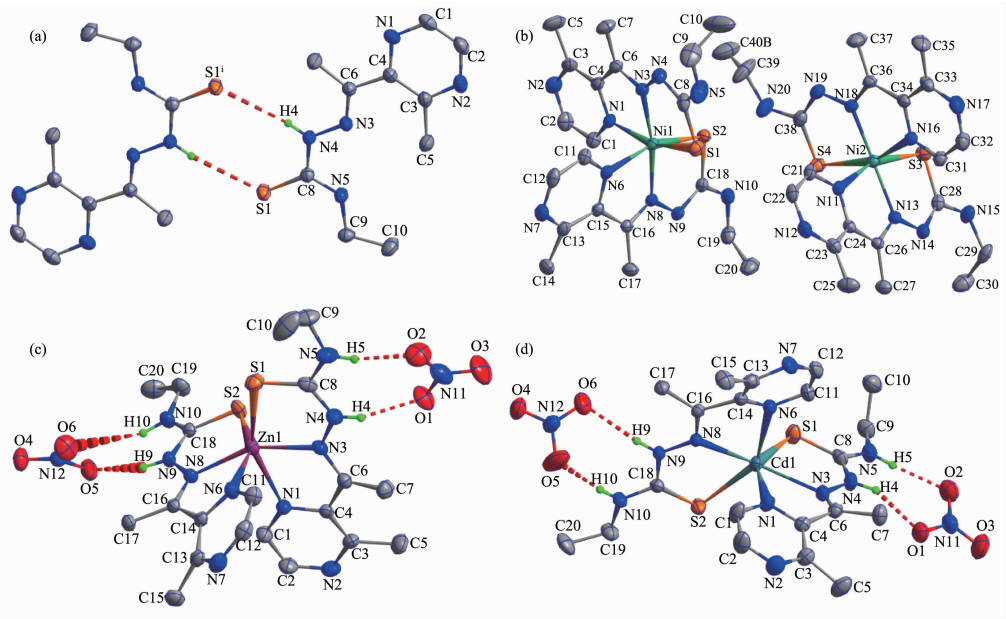

Symmetry codes: [i] $-x+2, -y+1, -z$; Hydrogen bonds are shown in dashed line

Fig.1 ORTEP drawing of HL (a) and complexes **1~3** (b~d) with 30% thermal ellipsoids

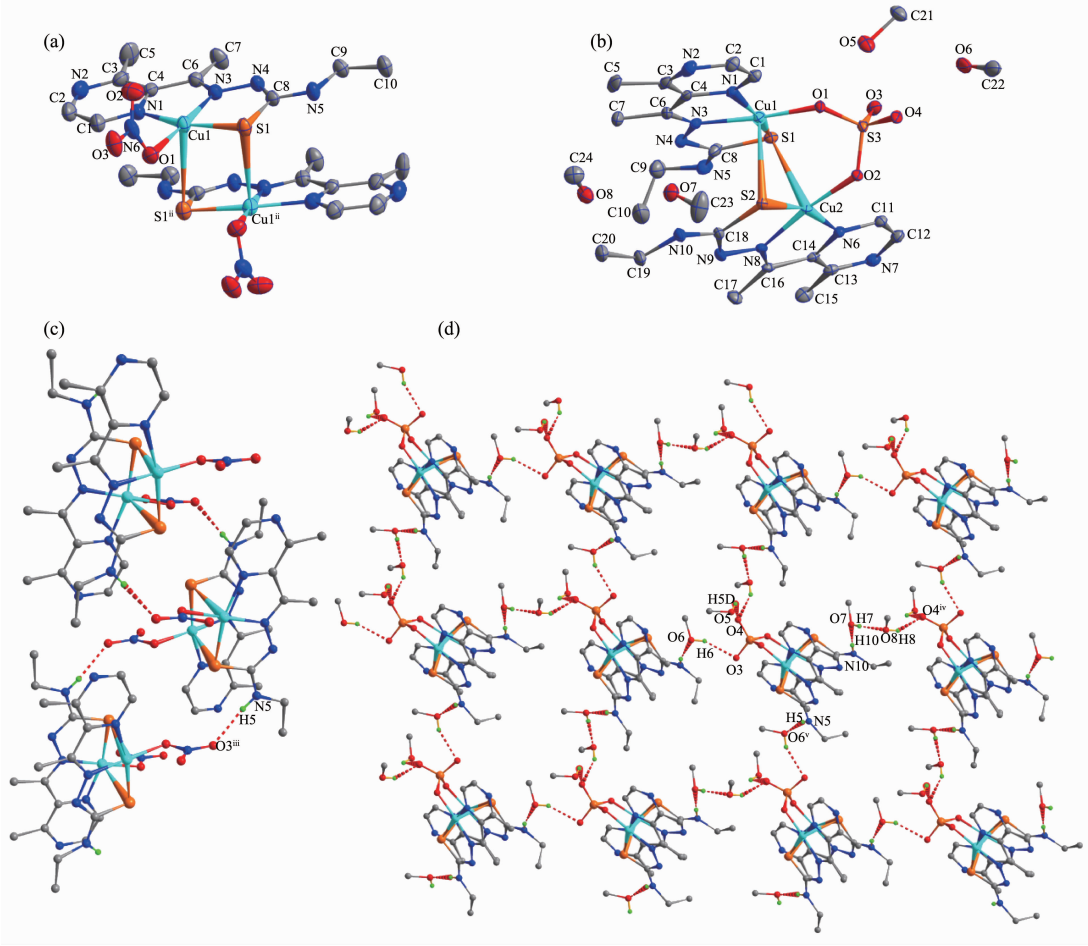

Symmetry codes: [ii] $-x, y, -z+0.5$; [iii] $x, -y, z-0.5$; [iv] $-x+1, y-0.5, -z+0.5$; [v] $-x+2, y-0.5, -z+1.5$

Fig.2 ORTEP drawing of complexes **4** (a) and **5** (b) with 30% thermal ellipsoids; Extended chain-like structure in the crystal of **4** (c) and 2D supramolecular structure in the crystal of **5** formed by hydrogen bonds shown in dashed line (d)

Table 2　Selected bond lengths (nm) and angles (°) for HL and complexes 1~5

			HL		
S1-C8	0.168 0(2)	N4-C8	0.137 2(3)	N5-C8	0.132 6(3)
			1		
Ni1-N1	0.207 7(3)	Ni1-N3	0.202 4(3)	Ni1-N6	0.210 9(3)
Ni1-N8	0.203 0(3)	Ni1-S1	0.240 32(12)	Ni1-S2	0.240 44(11)
Ni2-N16	0.207 0(3)	Ni2-N13	0.202 0(3)	Ni2-N11	0.210 8(3)
Ni2-N18	0.201 6(3)	Ni2-S3	0.240 14(11)	Ni2-S4	0.240 45(12)
N3-Ni1-N8	169.59(12)	N1-Ni1-N6	89.14(11)	N3-Ni1-S2	106.05(9)
N3-Ni1-N1	77.01(12)	N3-Ni1-S1	81.77(9)	N8-Ni1-S2	81.52(9)
N8-Ni1-N1	95.83(12)	N8-Ni1-S1	104.95(8)	N1-Ni1-S2	92.16(8)
N3-Ni1-N6	94.78(11)	N1-Ni1-S1	158.70(9)	N6-Ni1-S2	158.89(8)
N8-Ni1-N6	77.39(11)	N6-Ni1-S1	90.84(8)	S1-Ni1-S2	95.44(4)
N18-Ni2-N13	170.79(12)	N16-Ni2-N11	89.95(11)	N18-Ni2-S4	82.23(9)
N18-Ni2-N16	77.20(12)	N18-Ni2-S3	105.34(9)	N13-Ni2-S4	103.30(8)
N13-Ni2-N16	96.80(12)	N13-Ni2-S3	81.55(9)	N16-Ni2-S4	159.28(9)
N18-Ni2-N11	94.96(11)	N16-Ni2-S3	91.27(8)	N11-Ni2-S4	89.36(8)
N13-Ni2-N11	77.91(11)	N11-Ni2-S3	159.43(9)	S3-Ni2-S4	96.57(4)
			2		
Zn1-N1	0.226 9(3)	Zn1-N3	0.215 4(3)	Zn1-N6	0.220 7(3)
Zn1-N8	0.215 9(3)	Zn1-S1	0.244 35(14)	Zn1-S2	0.242 36(13)
N3-Zn1-N8	155.43(12)	N6-Zn1-N1	86.05(13)	N3-Zn1-S1	80.34(10)
N3-Zn1-N6	94.73(12)	N3-Zn1-S2	112.38(9)	N8-Zn1-S1	120.52(9)
N8-Zn1-N6	72.63(12)	N8-Zn1-S2	79.97(9)	N6-Zn1-S1	93.48(10)
N3-Zn1-N1	71.31(12)	N6-Zn1-S2	152.25(9)	N1-Zn1-S1	151.49(9)
N8-Zn1-N1	86.56(12)	N1-Zn1-S2	96.77(9)	S2-Zn1-S1	96.71(5)
			3		
Cd1-N1	0.242 2(3)	Cd1-N3	0.235 7(3)	Cd1-N6	0.237 3(3)
Cd1-N8	0.236 4(3)	Cd1-S1	0.253 97(13)	Cd1-S2	0.253 29(13)
N3-Cd1-N8	148.82(11)	N6-Cd1-N1	82.87(12)	N3-Cd1-S1	76.14(8)
N3-Cd1-N6	96.38(11)	N3-Cd1-S2	118.14(9)	N8-Cd1-S1	130.07(8)
N8-Cd1-N6	67.55(11)	N8-Cd1-S2	75.96(8)	N6-Cd1-S1	96.05(9)
N3-Cd1-N1	66.72(11)	N6-Cd1-S2	143.19(8)	N1-Cd1-S1	142.41(8)
N8-Cd1-N1	84.34(10)	N1-Cd1-S2	98.57(9)	S2-Cd1-S1	103.91(4)
			4		
Cu1-N1	0.200 4(4)	Cu1-N3	0.194 6(4)	Cu1-O1	0.197 7(3)
Cu1-S1	0.225 06(14)	Cu1-S1^{ii}	0.297 3		
N3-Cu1-O1	177.73(16)	O1-Cu1-N1	99.12(14)	O1-Cu1-S1	95.03(10)
N3-Cu1-N1	80.30(15)	N3-Cu1-S1	85.46(11)	N1-Cu1-S1	165.62(12)
			5		
Cu1-N1	0.200 7(5)	Cu1-N3	0.194 4(6)	Cu1-O1	0.192 7(4)
Cu1-S1	0.226 1(2)	Cu1-S2	0.278 1(3)	Cu2-N6	0.200 6(5)
Cu2-N8	0.192 7(5)	Cu2-O2	0.195 1(4)	Cu2-S1	0.274 4(2)
Cu2-S2	0.225 6(2)				

Continued Table 1

O1-Cu1-N3	173.4(2)	O1-Cu1-N1	94.0(2)	N3-Cu1-N1	79.8(3)
N1-Cu1-S1	163.02(18)	N1-Cu1-S2	92.91(17)	O1-Cu1-S1	99.80(13)
O1-Cu1-S2	90.62(15)	S1-Cu1-S2	96.81(7)	N3-Cu1-S1	86.0(2)
N3-Cu1-S2	91.91(19)	S2-Cu2-S1	97.97(7)	N8-Cu2-O2	172.5(2)
N8-Cu2-S2	86.13(18)	N8-Cu2-S1	90.89(18)	N8-Cu2-N6	80.2(2)
O2-Cu2-S2	96.43(13)	O2-Cu2-S1	95.67(16)	O2-Cu2-N6	95.9(2)
N6-Cu2-S2	162.75(18)	N6-Cu2-S1	92.80(17)		

Symmetry codes: [ii] $-x$, y, $-z+0.5$

Table 3 Hydrogen bond parameters for HL and complexes 2~5

D–H···A	d(D-H) / nm	d(H···A) / nm	d(D···A) / nm	∠DHA / (°)
		HL		
N4–H4···S1[i]	0.086	0.274	0.359 7(3)	171.8
		2		
N9–H9···O6	0.086	0.245	0.319 1(5)	145.2
N10–H10···O5	0.086	0.203	0.286 0(5)	163.5
N4–H4···O1	0.086	0.203	0.281 6(5)	151.6
N5–H5···O2	0.086	0.203	0.287 9(6)	167.8
		3		
N9–H9···O6	0.086	0.215	0.294 9(5)	153.4
N10–H10···O5	0.086	0.193	0.279 1(5)	173.6
N4–H4···O1	0.086	0.205	0.282 5(5)	148.9
N5–H5···O2	0.086	0.201	0.286 0(5)	169.2
		4		
N5–H5···O3[iii]	0.086	0.209	0.294 3(5)	171.2
		5		
O5–H5D···O4	0.082	0.245	0.291 2(8)	116
O7–H7···O8	0.082	0.195	0.271 3(9)	154
O8–H8···O4[iv]	0.082	0.203	0.279 1(9)	155
N5–H5···O6[v]	0.086	0.204	0.286 5(11)	161
N10–H10···O7	0.086	0.204	0.290 2(9)	176
O6–H6···O3	0.082	0.220	0.296 8(9)	156

Symmetry codes: [i] $-x+2$, $-y+1$, $-z$; [iii] x, $-y$, $z-0.5$; [iv] $-x+1$, $y-0.5$, $-z+0.5$; [v] $-x+2$, $y-0.5$, $-z+1.5$

ligands with N_2S donor sets. The distances of Ni-N/S bonds are in a range of 0.201 6(3)~0.240 45(12) nm and are similar as those found in some reported complexes[18]. As expected, there is no classic hydrogen bonds in the crystal.

Complex **2** and **3** are isostructural, thus complex **2** is discussed for example. In complex **2** (Fig.1b), the Zn(Ⅱ) ion is coordinated by two neutral TSC ligands with N_2S donor sets, and thus possesses a distorted octahedron coordination geometry. There are two free nitrate anions in the outside of the complex for charge balance. In addition, intermolecular N–H···O hydrogen bonds between the complex cations and free nitrate anions could be observed in the crystals of **2** and **3**.

Complex **4** crystallizes in a monoclinic space group $C2/c$, with one discrete dimeric Cu(Ⅱ) unit in the unit cell. As illustrated in Fig.2a, two Cu ions of the dimer are separated by 0.339 3 nm and doubly bridged by two S atoms of two TSC ligands to form a nearly planar four-membered Cu_2S_2 core. Each of the Cu(Ⅱ) ions is penta-coordinated by two S atoms from two different TSC ligands, two nitrogen atoms from

one TSC ligand and one terminal bromide, giving a distorted square pyramid coordination geometry (τ= 0.202). The distances of Cu-N/S bonds (0.194 6(4)~ 0.297 3 nm) are in good agreement with the corresponding distances reported in literature[18]. In solid state, the discrete Cu (Ⅱ) dimers of **4** are further linked into a one-dimensional chain along *c* axis (Fig.2c) by intermolecular N–H···O hydrogen bonds.

X-ray analysis of **5** revealed that it also has a dimeric unit consisting of two Cu(Ⅱ), one SO_4^{2-} ion and two TSC ligands, together with four crystal methanol molecules; it crystallizes in a monoclinic system with space group $P2_1/c$. As shown in Fig.2b, the coordination geometry around Cu (Ⅱ) in the dimeric complex is structurally similar to that of complex **4** (τ=0.169 and 0.164 in the case of Cu1 and Cu2, respectively); the only difference is the presence of a μ_2-SO_4^{2-} at the outer axial sites on both Cu (Ⅱ) ions. The four-membered Cu_2S_2 core and the Cu-S distances (0.225 74(19) and 0.274 4(2) nm) are also similar to those found in complex **4**. In the crystal, a large amount of intermolecular N–H···O and O–H···O hydrogen bonds link the molecules into a 2D supramolecular network (Fig.2d).

2.2 IR spectra

The most useful infrared spectral bands for determining the mode of coordination of ligands are the $\nu_{N=C}$, $\nu_{N=C}$ (pyrazine), and $\nu_{S=C}$ vibrations. The $\nu_{N=C}$ band of the TSC ligand was found at 1 608 cm^{-1}, while it shifted to 1 571~1 593 cm^{-1} in complexes **1~5**. The decrease in frequency of this band is an evidence for the coordination via the imine nitrogen atom[13,20]. In the TSC ligand, a band at 1 553 cm^{-1} is assigned to $\nu_{N=C}$(pyrazine), whereas this band was found to shift to 1 533~1 536 cm^{-1} in complexes **1~5**, confirming that pyrazine nitrogen atom takes part in coordination[13]. The $\nu_{S=C}$ vibration at 813 cm^{-1} in the TSC ligand shifted to lower frequency in the complexes, indicating the coordination of sulfur to the metal ions center[20]. Additionally, bands at about 1 384 cm^{-1} indicate that free nitrate groups exist in complexes **2** and **3**. Two intense absorption bands in the spectra of complex **4** associated with the asymmetric stretching appeared at 1 474 (ν_1) and 1 343 cm^{-1} (ν_4), establishing that the coordinated NO_3^- groups are monodentate ligands[20]. It is in accordance with the results of crystal structure analysis.

2.3 UV spectra

The UV spectra of the ligand HL, complexes **1~5** in CH_3OH solution (c=10 μmol·L^{-1}) were measured at room temperature (Fig.3). The spectrum of HL featured only one main band located around 308 nm (ε= 31 806 L·mol^{-1}·cm^{-1}), which could be contributed to the characteristic π-π* transition of pyrazine[13]. Similar bands were observed at 316 nm (ε=23 565 L·mol^{-1}·cm^{-1}), 311 nm (ε=24 696 L·mol^{-1}·cm^{-1}), 310 nm (ε= 25 541 L·mol^{-1}·cm^{-1}), 311 nm (ε=32 955 L·mol^{-1}·cm^{-1}) and 310 nm (ε=30 138 L·mol^{-1}·cm^{-1}) in complexes **1 ~5**, respectively. However, there were new bands at 437 nm (ε=8 209 L·mol^{-1}·cm^{-1}), 416 nm (ε= 15 071 L·mol^{-1}·cm^{-1}), 404 nm (ε=13 447 L·mol^{-1}·cm^{-1}), 438 nm (ε=17 712 L·mol^{-1}·cm^{-1}) and 438 nm (ε =12 909 L·mol^{-1}·cm^{-1}) in the complexes **1 ~5**, respectively, probably due to the ligand-to-metal charge transfer (LMCT)[21]. All facts reveal the coordination of the ligand to the central metal ions.

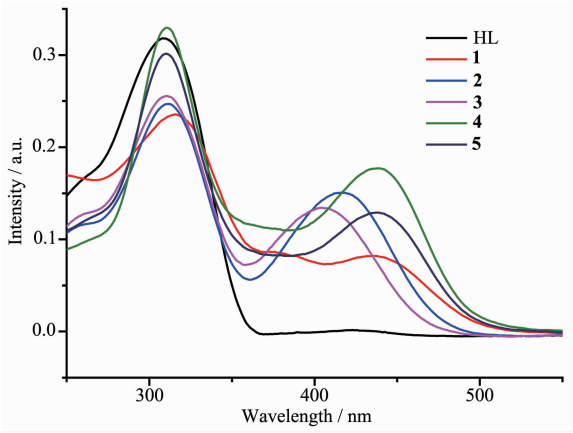

c=10 μmol·L^{-1}

Fig.3 UV spectra of ligand HL, complexes **1~5** in CH_3OH solution at room temperature

2.5 EB-DNA binding study by fluorescence spectrum

It is well known that EB can intercalate nonspecifically into DNA, which causes it to fluoresce strongly. Competitive binding of other drugs to DNA and EB will result in displacement of bound EB and a decrease in the fluorescence intensity[17]. The effects of

ligand HL and complexes **1**~**5** on the fluorescence spectra of EB-DNA system are presented in Fig.4. The fluorescence intensities of EB bound to ct-DNA at about 600 nm showed remarkable decreasing trends with the increasing concentration of tested compounds, indicating that some EB molecules are released into solution after the exchange with the compounds. The quenching of EB bound to DNA by the compounds is in agreement with the linear Stern-Volmer equation: $I_0/I=1+K_{sq}r$[19], where I_0 and I represent the fluorescence intensities in the absence and presence of quencher, respectively; K_{sq} is the linear Stern-Volmer quenching constant, r is the ratio of the concentration of quencher and DNA. In the quenching plots of I_0/I versus r, K_{sq} values are given by the slopes. The K_{sq} values are 1.069, 0.824, 0.752, 0.947 and 1.107 for complexes **1**~**5**, respectively, while that of the ligand HL is tested to be 0.587. The results indicate that the interactions of complexes **1**~**5** with DNA are stronger than that of ligand HL, which may be explained by the higher rigidity of the complexes to bind the base pairs along DNA[22]. The Ni(Ⅱ) complex **1**, and Cu(Ⅱ) complexes **4** and **5** displayed higher DNA interaction abilities than those of **2** and **3**, indicating that the type of

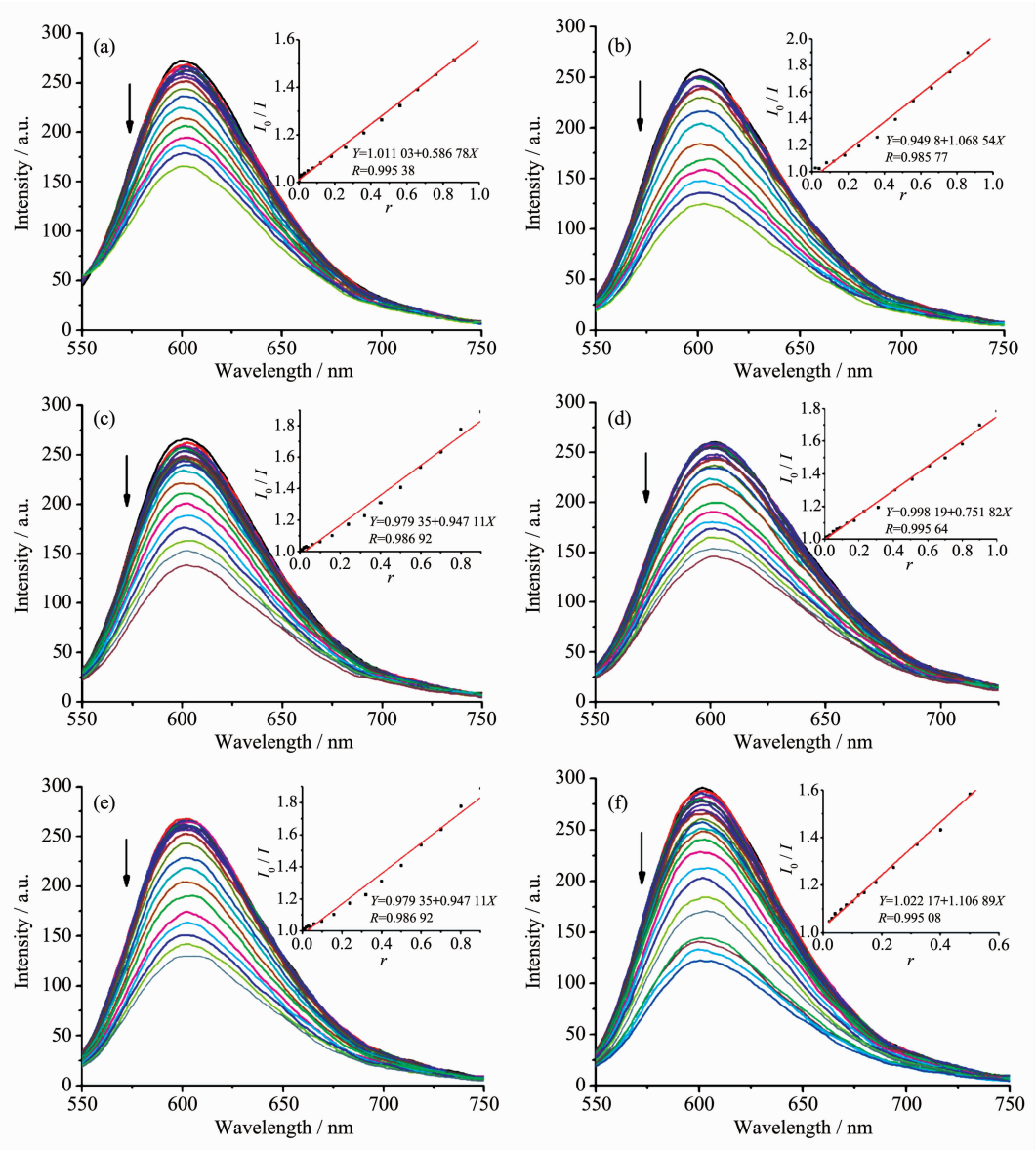

Arrow shows the fluorescence intensities change of EB-DNA system upon increasing tested compound concentration; Inset: plot of I_0/I versus r

Fig.4 Emission spectra of EB-DNA system in the absence and presence of ligand HL (a) and complexes **1**~**5** (b~f), respectively

metal centers are responsible for the properties in some content.

3 Conclusions

Five transition metal complexes with a pyrazine-containing thiosemicarbazone ligand were prepared and characterized by single-crystal X-ray crystallography. Moreover, the fluorescence spectra indicate that the interactions between the complexes and DNA are stronger than that of ligand HL, especially the Ni(Ⅱ) complex **1**, and the dimeric Cu(Ⅱ) complexes **4** and **5**, indicating that the type of metal centers are responsible for the properties in some content. Further research is needed to better determine the relationship between structures and activities.

References:

[1] Beraldo H, Gambino D. *Mini-Rev. Med. Chem.*, **2014**,**4**:31-39

[2] Wang Y T, Fang Y, Zhao M, et al. *Med. Chem. Commun.*, **2017**,**8**:2125-2132

[3] Qi J X, Deng J G, Qian K, et al. *Eur. J. Med. Chem.*, **2017**, **134**:34-42

[4] Qi J X, Liang S C, Gou Y, et al. *Eur. J. Med. Chem.*, **2015**, **96**:360-368

[5] Qi J X, Zheng Y Y, Qian K, et al. *J. Inorg. Biochem.*, **2017**, **177**:110-117

[6] Zeglis B M, Divilov V, Lewis J S. *J. Med. Chem.*, **2011**,**54**: 2391-2398

[7] Li M X, Zhang L Z, Yang M, et al. *Bioorg. Med. Chem. Lett.*, **2012**,**22**:2418-2423

[8] Li M X, Chen C L, Zhang D, et al. *Eur. J. Med. Chem.*, **2010**,**45**:3169-3177

[9] Rogolino D, Cavazzoni A, Gatti A, et al. *Eur. J. Med. Chem.*, **2017**,**128**:140-153

[10]Lovejoy D B, Sharp D M, Seebacher N, et al. *J. Med. Chem.*, **2012**,**55**:7230-7244

[11]Matesanz A I, Leitao I, Souza P. *J. Inorg. Biochem.*, **2013**, **125**:26-31

[12]Matesanz A I, Souza P. *Inorg. Chem. Commun.*, **2013**,**27**:5-8

[13]WU Hao(吴浩), WANG Yuan(王元), SONG Yu-Fei(宋雨飞), et al. *Chinese J. Inorg. Chem.*(无机化学学报), **2018**, **34**:2057-2062

[14]Ramachandran E, Thomas S P, Poornima P, et al. *Eur. J. Med. Chem.*, **2012**,**50**:405-415

[15]Sheldrick G M. *SADABS*, University of Göttingen, Germany, **1996**.

[16]Sheldrick G M. *SHELX*-97, *Program for the Solution and the Refinement of Crystal Structures*, University of Göttingen, Germany, **1997**.

[17]MAO Pan-Dong(毛盼东), YAN Ling-Ling(闫玲玲), WANG Wen-Jing(王文静), et al. *Chinese J. Inorg. Chem.*(无机化学学报), **2016**,**32**:555-560

[18]Hangan A C, Borodi G, Stan R L, et al. *Inorg. Chim. Acta*, **2018**,**482**:884-893

[19]MAO Pan-Dong(毛盼东), HAN Xue-Feng(韩学锋), WU Wei-Na(吴伟娜), et al. *Chinese J. Inorg. Chem.*(无机化学学报), **2016**,**32**:161-166

[20]Nakamoto K. *Infrared and Raman Spectra of Inorganic and Coordination Compounds*. 4*th Ed*. New York: Wiley, **1986**: 257

[21]Mahjoobizadeh M, Takjoo R, Farhadipour A, et al. *Inorg. Chim. Acta*, **2018**,**482**:643-653

[22]Kalaiarasi G, Dharani S, Puschmann H, et al. *Inorg. Chem. Commun.*, **2018**,**97**:34-38